Optical activity of metallic helices in the terahertz domain: a theoretical investigation

François Hache* and Guilhem Gallot

Laboratoire d'Optique et Biosciences, CNRS-INSERM Ecole Polytechnique, 91128 Palaiseau cedex, France
**Corresponding author: francois.hache@polytechnique.edu*

Received May 15, 2012; revised July 10, 2012; accepted July 11, 2012;
posted July 13, 2012 (Doc. ID 168598); published September 6, 2012

Optical activity in the terahertz spectral domain has recently seen a growing interest, but fine understanding of these phenomena is not yet developed. In this article, we study analytically the response of a metallic helix in the terahertz regime and present a full nonlocal calculation of its chiroptical response. Because we do not use multipolar expansion, this calculation is very general and applies to the case where the helix size is comparable to the wavelength of the light. We calculate the circular birefringence and dichroism in three configurations: propagation along or perpendicular to the helix axis and response of an isotropic distribution of such helices. We obtain analytical expressions and can examine the consequence of the breakdown of the multipolar expansion and the wavelength-dependence of the chiroptical response, as well as give orders of magnitude that compare favorably with experimental data. This calculation is also comforted by a finite element calculation.

OCIS codes: 260.2130, 260.3910, 300.6495.

1. INTRODUCTION

Terahertz spectroscopy has seen a very important development in the last decade and thanks to the progress in experimental techniques, more and more fundamental aspects of this wavelength range have been studied [1]. Terahertz radiation lies between microwaves and infrared optics and extension of the principles of optics in this region is not straightforward, in particular because usual approximation of optics may not be valid any longer. Among the optical properties well-studied in optics whose extension in the terahertz regime is not fully achieved, the optical activity has received lately some attention [2,3]. In particular, Chau has measured the circular birefringence of a 12-turn helix whose characteristic size is comparable with terahertz radiation wavelengths [4]. He measured a noticeable variation of the refractive index for left- and right-circular polarizations.

Circular birefringence in optics is well accounted for by introducing the Rosenfeld rotational strength, which scales as a dot product between an electric dipole moment and a magnetic one [5]. This calculation relies on a multipolar expansion of the light–matter interaction. Usual dipole approximation amounts to neglecting the size of the systems under study compared to the light wavelength. Although fully justified when comparing the orders of magnitude, this local approximation does not allow one to introduce chiroptical effects because such effects originate in the three-dimensional (3D) structure of the systems, which are accessible only in a nonlocal treatment where the propagating character of the electromagnetic wave is conserved. The easiest way to introduce nonlocal response is therefore to use a first-order multipolar expansion, $e^{ikr} = 1 + ikr$, or equivalently to introduce magnetic dipolar and electric quadrupolar responses. However, this expansion is justified only for systems much smaller than the wavelength [6]. Such is not the case in the issue we are interested in here. In Chau's paper, the helix dimensions are comparable to the wavelength and the multipolar expansion is not expected to converge. It is therefore necessary to introduce the optical response of these systems in a fully nonlocal manner, without any multipolar expansions [7]. Formal introduction of a nonlocal dielectric function has already been proposed. For example, Wood and Ashcroft introduced this nonlocal dielectric function to study the optical response of small metallic quantum dots [8]. In this article, we propose to derive an exact calculable expression of the circular birefringence of a metallic helix starting from the general expression of the nonlocal dielectric function introduced in [8] and utilizing the model of free electrons on a helix as proposed in [9].

The dielectric constant of the material will therefore be calculated in the fully nonlocal framework, without any assumption about the relative magnitude of the wavelength and of the geometrical dimension of the helices. For that purpose, we carry out a complete quantum calculation in the general framework where the electromagnetic field interacts with the matter through its potential vector instead of its electric and magnetic fields as usually done. We will show that in the limit of a long helix, we obtain analytical expressions for an electromagnetic field impinging perpendicular or parallel to the helix axis. These expressions allow us to obtain the circular birefringence as well as the circular dichroism for an assembly of helices either oriented in a unique direction or isotropically distributed.

Following this calculation, three aspects will be discussed: (i) the consequence of the breakdown of the commonly used multipolar expansion, in particular for the chiral signals of an isotropic distribution of helices, (ii) the wavelength-dependence of the chiroptical response in the terahertz regime, and (iii) the comparison of the numerical estimate of the circular birefringence with the one measured in Chau's experiment. Finally, we will also briefly present a finite

element calculation that brings another point of view and comforts numerically our theoretical developments.

2. NONLOCAL DIELECTRIC FUNCTION

In this section, we want to establish the general expression of the fully nonlocal dielectric tensor. Since the separation of the electric and magnetic response is not meaningful in the fully nonlocal description, we work in the Landau–Lifchitz approach [7,10], which encompasses all the microscopic currents induced by the electromagnetic field into a nonlocal dielectric function $\varepsilon(\mathbf{k},\omega)$. We start by deriving the general expression of the nonlocal dielectric function, which we will apply in the following sections to the specific case of a metallic helix.

Let us consider a quantum system depicted by a Hamiltonian $\widehat{H}_0$ whose quantum states are denoted $|n\rangle$. When this system is irradiated by an electromagnetic wave of frequency ω, the total Hamiltonian becomes

$$\widehat{H} = \widehat{H}_0 + \widehat{H}_I, \tag{2.1}$$

where the interaction Hamiltonian can be expressed as a function of the momentum operator $\widehat{\mathbf{p}}$ and the vector potential $\mathbf{A}$:

$$\widehat{H}_I = \frac{e}{2m_e c}(\widehat{\mathbf{p}}\cdot\mathbf{A} + \mathbf{A}\cdot\widehat{\mathbf{p}}). \tag{2.2}$$

Note that we stick to the semiclassical approximation and that $\mathbf{A}$ is not an operator, but only a complex time- and space-dependent vector.

The electric current can be obtained from the electric current operator

$$\widehat{\mathbf{j}} = -\frac{e}{2m_e}[\widehat{n}(\mathbf{r})\widehat{\mathbf{p}}_c + \widehat{\mathbf{p}}_c\widehat{n}(\mathbf{r})] \tag{2.3}$$

with $\widehat{\mathbf{p}}_c = \widehat{\mathbf{p}} + \frac{e}{c}\mathbf{A}$ and $\widehat{n}(\mathbf{r}) = \delta(\mathbf{r}-\widehat{\mathbf{r}})$ and the density matrix by

$$\mathbf{j} = \mathrm{Tr}[\widehat{\rho}\widehat{\mathbf{j}}]. \tag{2.4}$$

Actually, this induced current is comprised of two contributions. On the one hand, the electromagnetic field will induce a current in the unperturbed electric distribution, as it appears in the dependence of $\widehat{\mathbf{j}}$ with $\mathbf{A}$, which reads

$$\mathbf{j}_0 = -\frac{e^2}{m_e c}\mathrm{Tr}[\widehat{\rho}^{(0)}\widehat{n}]\mathbf{A}. \tag{2.5}$$

On the other hand, the electronic distribution itself is perturbed by the electromagnetic fields and a first-order perturbed distribution $\widehat{\rho}^{(1)}$ appears. This yields an extra current given by

$$\mathbf{j}_1 = -\frac{e}{2m_e}\mathrm{Tr}[\widehat{\rho}^{(1)}(\widehat{n}\,\widehat{\mathbf{p}} + \widehat{\mathbf{p}}\,\widehat{n})]. \tag{2.6}$$

Calculation of $\mathbf{j}_0$ straightforwardly yields the Drude dielectric constant. Making explicit the Trace operation in Eq. (2.5) yields, with $\mathbf{A} = \mathbf{A}_0 e^{i(\mathbf{k}\cdot\mathbf{r}-\omega t)}$,

$$\begin{aligned}\mathbf{j}_0(\mathbf{r},t) &= -\frac{e^2}{m_e c}\sum_{m,n}\langle n|\widehat{\rho}^{(0)}|m\rangle\langle m|\widehat{n}\mathbf{A}|n\rangle \\ &= -\frac{e^2}{m_e c}\mathbf{A}_0 e^{-i\omega t}\sum_m f_m\langle m|e^{i\mathbf{k}\cdot\widehat{\mathbf{r}}}\widehat{n}(\mathbf{r})|m\rangle.\end{aligned} \tag{2.7}$$

f_m is the occupation number of the state $|m\rangle$ (energy E_m), given by the Fermi–Dirac distribution (with E_F the Fermi energy):

$$f_m = \frac{1}{\exp\left(\frac{E_m - E_F}{k_B T}\right) + 1}. \tag{2.8}$$

The total number of electrons is $N = \sum_m f_m$. Here, the current is defined in the real space. However, it is necessary to go to the reciprocal space in order to define the conductivity. This is achieved by defining the space Fourier transform on a volume Ω by

$$g(\mathbf{k}') = \frac{1}{\Omega}\int f(\mathbf{r})e^{-i\mathbf{k}'\cdot\mathbf{r}}d\mathbf{r}. \tag{2.9}$$

We therefore calculate for the ω component,

$$\mathbf{j}_0(\mathbf{k}',\omega) = -\frac{e^2}{\Omega m_e c\omega}\mathbf{A}_0\sum_m f_m\langle m|e^{i(\mathbf{k}-\mathbf{k}')\cdot\widehat{\mathbf{r}}}|m\rangle. \tag{2.10}$$

This expression yields a very general form of nonlocal current. For a homogeneous system, only the diagonal terms for which $\mathbf{k}' = \mathbf{k}$ are nonzero [8], and we have

$$\mathbf{j}_0(\mathbf{k},\omega) = -\frac{Ne^2}{\Omega m_e c}\mathbf{A}_0, \tag{2.11}$$

where we have introduced N the total number of electrons in the volume Ω. Introducing a relaxation term Γ (the reader is referred to [8] for a thorough discussion of this factor), we can readily express the conductivity [11]

$$\sigma(\omega) = i\frac{Ne^2}{\Omega m_e(\omega + i\Gamma)}, \tag{2.12}$$

which is found to be independent of $\mathbf{k}$. From this expression, we calculate the dielectric tensor, which reduces to a constant

$$\varepsilon(\omega) = 1 - \frac{\omega_p^2}{\omega(\omega+i\Gamma)} \quad \text{with } \omega_p^2 = \frac{Ne^2}{\Omega m_e \varepsilon_0}, \tag{2.13}$$

and we recover the well-known formula with the plasma frequency ω_p.

This formula allows one to understand the behavior of an electromagnetic wave in a metal [11]. For $\omega < \omega_p$, the real part of the dielectric constant is negative, which prevents propagation of the wave inside the metal. However, it is well-known that this is not perfectly true near the surface and that the electromagnetic field exponentially decays within the "penetration depth" or "skin thickness" given by [12]

$$d = \frac{1}{\sqrt{\pi f\mu\sigma}}, \tag{2.14}$$

where f is the frequency and μ is the permeability. At $f = 1$ THz, the conductivity of copper [13] is $\sigma = 5.96\times 10^7$ S/m, and one obtains $d \approx 65$ nm.

This description is, however, not sufficient to account for any chiral effect in metallic helices. Indeed, the electric current is proportional to the electric field ($\sigma(\omega)$ is a scalar) and no different behaviors are expected for a left- or a right-circular polarization. It is therefore necessary to go further in the perturbative action of the electromagnetic field and to consider the $\mathbf{j}_1$ term. To do so, we closely follow the derivation proposed in [8]. The evolution equation of the density matrix is

$$i\hbar\frac{\partial\widehat{\rho}}{\partial t} = [\widehat{H},\widehat{\rho}]. \tag{2.15}$$

At the first order in the applied electromagnetic field, this equation reads

$$i\hbar\frac{\partial\widehat{\rho}^{(1)}}{\partial t} = [\widehat{H}_I,\widehat{\rho}^{(0)}] + [\widehat{H}_0,\widehat{\rho}^{(1)}]. \tag{2.16}$$

Resolution of this equation yields the first-order density matrix elements

$$\langle n|\widehat{\rho}^{(1)}|m\rangle = \frac{f_n - f_m}{\hbar(\omega_{nm} - \omega - i\Gamma)}\langle n|\widehat{H}_I|m\rangle, \tag{2.17}$$

where $\hbar\omega_{nm}$ is the energy difference between the two levels and where we have also introduced a linewidth Γ. Introducing the expression of the interaction Hamiltonian with $\mathbf{A} = \mathbf{A}_0 e^{i(\mathbf{k}\cdot\mathbf{r}-\omega t)}$, one obtains

$$\langle n|\widehat{H}_I|m\rangle = \frac{e}{2m_e c}\mathbf{A}_0\cdot[\langle n|e^{i\mathbf{k}\cdot\widehat{\mathbf{r}}}\widehat{\mathbf{p}}|m\rangle + \langle n|\widehat{\mathbf{p}}e^{i\mathbf{k}\cdot\widehat{\mathbf{r}}}|m\rangle]e^{-i\omega t}, \tag{2.18}$$

or, making explicit the Trace operation,

$$\mathbf{j}_1(\mathbf{r},t) = -\frac{e}{2m_e}\sum_{m,n}\langle n|\widehat{\rho}^{(1)}|m\rangle\langle m|\widehat{n}(\mathbf{r})\widehat{\mathbf{p}} + \widehat{\mathbf{p}}\,\widehat{n}(\mathbf{r})|n\rangle. \tag{2.19}$$

Inserting the expression calculated for $\widehat{\rho}^{(1)}$, we obtain

$$\begin{aligned}\mathbf{j}_1(\mathbf{r},t) = &-\frac{e^2}{2m_e^2 c}\sum_{m,n}\frac{f_n - f_m}{\hbar(\omega_{nm} - \omega - i\Gamma)}\mathbf{A}_0\\ &\cdot[\langle n|e^{i\mathbf{k}\cdot\widehat{\mathbf{r}}}\widehat{\mathbf{p}}|m\rangle + \langle n|\widehat{\mathbf{p}}e^{i\mathbf{k}\cdot\widehat{\mathbf{r}}}|m\rangle]\\ &\times[\langle m|\widehat{n}(\mathbf{r})\widehat{\mathbf{p}}|n\rangle + \langle m|\widehat{\mathbf{p}}\,\widehat{n}(\mathbf{r})|n\rangle]e^{-i\omega t}.\end{aligned} \tag{2.20}$$

Note that only the brackets in the last line are functions of the position $\mathbf{r}$. Applying the Fourier transform to this expression and sticking to the diagonal response approximation therefore allows us to define a nonlocal conductivity by

$$\begin{aligned}\underline{\underline{\sigma_1}}(\mathbf{k},\omega) = &\, i\frac{e^2}{2\Omega m_e^2\omega}\sum_{m,n}\frac{f_n - f_m}{\hbar(\omega_{nm} - \omega - i\Gamma)}\\ &\times[\langle m|e^{-i\mathbf{k}\cdot\widehat{\mathbf{r}}}\widehat{\mathbf{p}}|n\rangle + \langle m|\widehat{\mathbf{p}}e^{-i\mathbf{k}\cdot\widehat{\mathbf{r}}}|n\rangle]\\ &\times[\langle n|e^{i\mathbf{k}\cdot\widehat{\mathbf{r}}}\widehat{\mathbf{p}}|m\rangle + \langle n|\widehat{\mathbf{p}}e^{i\mathbf{k}\cdot\widehat{\mathbf{r}}}|m\rangle].\end{aligned} \tag{2.21}$$

This expression is quite general. It gives the nonlocal conductivity tensor without any hypothesis on the relative size of the system compared to the wavelength. It contains all the induced current and encompasses the electric and magnetic contributions, as well as higher-order terms. The $e^{i\mathbf{k}\cdot\widehat{\mathbf{r}}}$ terms are kept as a whole. Developing these terms as powers of $\mathbf{k}\cdot\mathbf{r}$ would give the usual multipolar expansion. At zeroth order, the matrix elements reduce to the oscillator strength $|\langle m|\widehat{\mathbf{p}}|n\rangle|^2$. This extra conductivity is, for example, responsible for the extra relaxation due to quantum size effects in metal nanoparticles [14]. It is worth noting that the diagonal response approximation can be used in a confined medium as has been shown for a small metal particle with the specular reflection model [15]

From the conductivity, one can express the dielectric tensor as

$$\underline{\underline{\varepsilon_1}}(\mathbf{k},\omega) = \frac{i}{\varepsilon_0\omega}\underline{\underline{\sigma_1}}(\mathbf{k},\omega). \tag{2.22}$$

This extra dielectric function can be seen as the dielectric function of the electron gas of the helix submitted to the electromagnetic field. In other words, the $\mathbf{j}_0$ term yields a redistribution of the electron density to counteract the effect of the electric field, whereas the $\mathbf{j}_1$ term reveals the dielectric response of this perturbed electron distribution and allows us to define an extra effective dielectric tensor. Actually, this nonlocal response is very sensitive to the chirality of the system and yields an effective circular birefringence and dichroism through the nondiagonal terms of the dielectric tensor. For a light beam propagating in the X direction, the dielectric tensor $\underline{\underline{\varepsilon_1}}$ can be reduced to

$$\begin{pmatrix}\varepsilon_{YY} & \varepsilon_{YZ}\\ \varepsilon_{ZY} & \varepsilon_{ZZ}\end{pmatrix}. \tag{2.23}$$

Far from resonances, this matrix is a Hermitian matrix that can be diagonalized yielding the left- and right-circularly polarized beams as eigenmodes. The scalar dielectric constant for the two polarizations is given by

$$\varepsilon_\pm = \frac{1}{2}[(\varepsilon_{YY} + \varepsilon_{ZZ}) \pm i(\varepsilon_{YZ} - \varepsilon_{ZY})] \equiv \varepsilon_{iso} \pm \Delta\varepsilon. \tag{2.24}$$

The sign "+" (resp. "−") refers to the left- (resp. right-) handed polarization. ε_{iso} gives a small contribution to the regular dielectric constant, whereas $\Delta\varepsilon = \Im(\varepsilon_{YZ})$ is the unique chiral contribution. However, in the general case where absorption is present, $\Delta\varepsilon$ is a complex number: its real part yields the refractive index, whereas its imaginary part yields the absorption coefficient. One then obtains for the circular birefringence

$$\Delta n_c = \frac{\Re(\Delta\varepsilon)}{n_0}, \tag{2.25}$$

where n_0 is the effective refractive index of the composite medium and Δn_c is the difference in refractive index for a left- and a right-circular polarization, and for the circular dichroism

$$\Delta\alpha = \frac{2\omega\Im(\Delta\varepsilon)}{n_0 c}, \tag{2.26}$$

where ω is the light frequency and $\Delta\alpha$ is the difference in absorption coefficient for a left- and a right-circular polarization.

In the following, we will apply the general formula to our specific problem. From the above expressions, one can see

that one must calculate the nondiagonal components of the dielectric tensor to obtain the refractive index and the absorption coefficient.

3. MODEL: LONG FINITE HELIX

A. Eigenfunctions and Eigenenergies

In order to describe a metallic helix, we suppose that the electrons are free to evolve along a helical path as depicted in Fig. 1. Such a model has been introduced in [9]. The helix radius is a and the pitch is $2\pi b$. b is positive (resp. negative) for a left- (resp. right)-handed helix. We note $L^2 = a^2 + b^2$. The helix has K turns. Let us introduce a framework attached to the helix, x, y, z. The helix is supposed to begin and to terminate on the x axis. Therefore, the z axis is the same as the laboratory Z one, but the x, y can be rotated compared to the X, Y ones to allow for a random starting point of the helix in the laboratory frame. The position of the electrons in the helix frame can be marked with the angle θ:

$$x = a\cos\theta, \quad y = a\sin\theta, \quad z = b\theta.$$

The eigenfunctions can be easily determined by imposing that they go to 0 when $\theta = 0$ and $\theta = 2K\pi$:

$$\psi_l = \frac{1}{\sqrt{K\pi}}\sin l\theta \tag{3.1}$$

with the condition that $2Kl = p$ with p an integer number. The eigenenergies are then

$$E_l = l^2 E_0 \quad \text{with } E_0 = \frac{\hbar^2}{2m_e L^2}. \tag{3.2}$$

Note that l's are not integer numbers; however, energy quantization is ensured by the previous relation between l and the integer p. In this framework, the momentum operator is

$$p_x = i\frac{\hbar a}{L^2}\left[\sin\theta\frac{\partial}{\partial\theta} + \frac{1}{2}\cos\theta\right],$$
$$p_y = -i\frac{\hbar a}{L^2}\left[\cos\theta\frac{\partial}{\partial\theta} - \frac{1}{2}\sin\theta\right],$$
$$p_z = i\frac{\hbar b}{L^2}\frac{\partial}{\partial\theta}.$$

These expressions, calculated from the Lagrangian [9], ensure that the operators are Hermitian. The case of an infinite helix is the limiting case when $K \to \infty$.

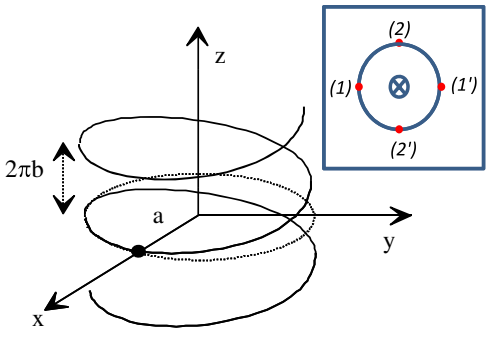

Fig. 1. (Color online) Sketch of the metallic helix. The framework x, y, z is attached to the helix. The inset represents a top view of the helix. The four outlined points (1), (1′), (2), (2′) are useful for the discussion.

B. Orders of Magnitude

Before proceeding to the calculation, it is worth giving some orders of magnitude of the various parameters. With the experimental parameters of Chau [4], $2a = 235\ \mu$m, $2\pi b = 120\ \mu$m, we calculate $L = 119\ \mu$m, which yields $E_0 = 2.7\times10^{-12}$ eV. Furthermore, the Fermi energy for copper being equal to 7 eV, we can calculate m_F, the index of the Fermi level: $E_F \equiv m_F^2 E_0$. This yields $m_F = 1.6\times10^6$. With those numbers, we can calculate that the smallest energy difference at the Fermi level, obtained for $\Delta m = 1$, is $\Delta E = 2m_F E_0 = 8.6\times10^{-6}$ eV, a very tiny value compared to a terahertz radiation (1 THz $\approx 4\times10^{-3}$ eV).

Another important piece of data is the copper electronic density ρ, which fixes the ratio N/Ω. However, it is not possible to extract N or Ω from the helix geometrical parameters for two reasons. First, because of the limited penetration of the electromagnetic field inside the metal (skin depth effect), the effective volume is not known. Second, in the present model we replace a 3D helix by a one-dimensional (1D)-helical path for the electrons and we ignore the other two dimensions. In the forthcoming calculation, the important parameter that will appear is the number of electrons that can fit the quantum space defined by our model. Remembering that $2Km = p$ with p an integer number, there are $2Km_F$ quantum states in which one can have $N = 4Km_F$ electrons, including the spin degeneracy. This number of electrons in turn fixes the effective volume in our calculation. *In fine*, the only relevant parameter is $\rho = 8.47\times10^{28}$ m^{-3}, as is already the case for the bulk dielectric constant [see Eq. (2.13)].

4. CALCULATION OF THE DIELECTRIC CONSTANT

For the sake of generality, we will consider two geometries. First, the propagation direction is assumed to be perpendicular to the helix axis in the X direction. However, as we have noticed above, it can correspond to a random orientation in the x, y frame. Considering that the polarization is in the YZ plane, the relevant dielectric constant is therefore $\varepsilon_{YZ} = \frac{1}{2}(\varepsilon_{xz} + \varepsilon_{yz})$. Second, we will consider the case where the propagation is parallel to the helix axis, namely the Z direction. In this case, the relevant dielectric tensor component is $\varepsilon_{XY} = \varepsilon_{xy}$. We will now calculate these tensor components in the framework of our model.

A. ε_{zx} Component

Let us note

$$A_{nm} = \langle n|e^{iky}\hat{p}_x|m\rangle,$$
$$B_{nm} = \langle n|e^{-iky}\hat{p}_z|m\rangle,$$
$$C_{nm} = [A_{nm} + (\tilde{A}_{mn})^*][B_{mn} + (\tilde{B}_{nm})^*],$$

where $\tilde{A}_{mn}$ and $\tilde{B}_{mn}$ are obtained from A_{mn} and B_{mn} by changing the k to $-k$. In this last expression, we used the identity $\langle m|\hat{\mathbf{p}}e^{-i\mathbf{k}\cdot\hat{\mathbf{r}}}|n\rangle = (\langle n|e^{i\mathbf{k}\cdot\hat{\mathbf{r}}}\hat{\mathbf{p}}|m\rangle)^*$. From the symmetry of this expression, one can easily check that $\varepsilon_{xz} = \varepsilon_{zx}^*$ when $\Gamma = 0$. With these definitions, the dielectric constant can be expressed as

$$\varepsilon_{zx} = -\frac{e^2}{4\varepsilon_0\Omega m_e^2\omega^2}\sum_{m,n}\frac{f_n - f_m}{\hbar(\omega_{nm} - \omega - i\Gamma)}C_{nm}. \tag{4.1}$$

We will see in the appendix that $C_{nm} = C_{mn}$, which yields

$$\varepsilon_{zx} = -\frac{e^2}{4\varepsilon_0 \hbar \Omega m_e^2 \omega^2} \sum_{m,n} (f_m - f_n) C_{nm} \frac{\omega_{nm}}{(\omega + i\Gamma)^2 - \omega_{nm}^2}. \quad (4.2)$$

We can simplify this expression if we suppose that $\omega, \Gamma \gg \omega_{nm}$. In that case, the dielectric constant can be reduced to

$$\varepsilon_{zx} = -\frac{e^2}{4\varepsilon_0 \hbar \Omega m_e^2 \omega^2} \frac{1}{(\omega + i\Gamma)^2} \sum_{m,n} (f_m - f_n) C_{nm} \omega_{nm}. \quad (4.3)$$

The calculation of $\sum_{m,n}(f_m - f_n)C_{nm}\omega_{nm}$ is proposed in the appendix. As explained there, the Bessel functions involved in this expression will have appreciable value only if $n \simeq m$. This corresponds to levels very close in energy (see above), for which the condition $\omega, \Gamma \gg \omega_{nm}$ is fully justified. Equation (4.3) then reduces to

$$\varepsilon_{zx} = i \frac{\omega_p^2 E_F n_0}{2 m_e c} \frac{1}{\omega(\omega + i\Gamma)^2} \frac{a^2 b}{L^4} \mathcal{F}(ka). \quad (4.4)$$

In this latter expression, the function $\mathcal{F}$ is defined by

$$\mathcal{F}(x) = \frac{4}{x} \sum_{l \text{ odd}} l^2 J_l'(x) J_l(x). \quad (4.5)$$

It is sketched in Fig. 2. Its maximum is equal to 1. Note that if one reverses the helicity of the system by changing b to $-b$, the sign of ε_{xz} is reversed as expected for a chiral response.

In the limit $ka \to 0$, this expression reduces to

$$\varepsilon_{zx} = i \frac{\omega_p^2 E_F n_0}{2 m_e c} \frac{1}{\omega(\omega + i\Gamma)^2} \frac{a^2 b}{L^4}. \quad (4.6)$$

One can also check that $\varepsilon_{xz} = -\varepsilon_{zx}$. Because $\varepsilon_{yz} = 0$ (see the appendix), we switch now to the calculation of ε_{yx}.

B. ε_{yx} Component

For this component, the relevant quantities are

$$D_{nm} = \langle n | e^{ikz} \hat{p}_x | m \rangle,$$
$$E_{nm} = \langle n | e^{-ikz} \hat{p}_y | m \rangle,$$
$$F_{nm} = [D_{nm} + (\tilde{D}_{mn})^*][E_{mn} + (\tilde{E}_{nm})^*],$$

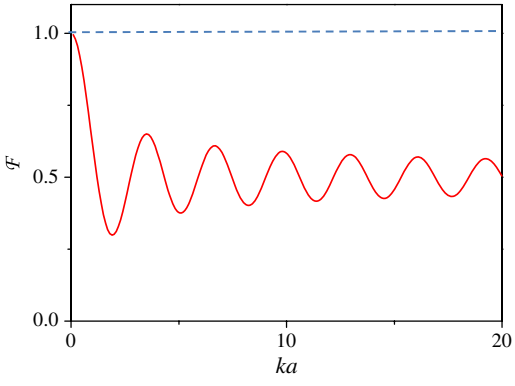

Fig. 2. (Color online) Functions $\mathcal{F}_\parallel$ (dashed line) and $F = -2\mathcal{F}_\perp$ (solid line) as a function of the parameter ka.

where $\tilde{D}_{mn}$ and $\tilde{E}_{mn}$ are obtained from D_{mn} and E_{mn} by changing the k to $-k$. With these definitions, and within the same approximations as above, the dielectric constant can be expressed as

$$\varepsilon_{yx} = -\frac{e^2}{4\varepsilon_0 \hbar \Omega m_e^2 \omega^2} \frac{1}{(\omega + i\Gamma)^2} \sum_{m,n} (f_m - f_n) F_{nm} \omega_{nm}. \quad (4.7)$$

The calculation of $\sum_{m,n} F_{nm}\omega_{nm}$ is proposed in the appendix, and we obtain an expression independent of k

$$\varepsilon_{yx} = -i \frac{\omega_p^2 E_F n_0}{2 m_e c} \frac{1}{\omega(\omega + i\Gamma)^2} \frac{a^2 b}{L^4}. \quad (4.8)$$

Here also, one has $\varepsilon_{xy} = -\varepsilon_{yx}$.

This expression is exactly equal to the opposite of Eq. (4.6). Indeed, the limit $ka \to 0$ corresponds to the local approximation and $\varepsilon_{xz} + \varepsilon_{zy} + \varepsilon_{yx}$ is proportional to the sum of the rotational strengths, which is known to be null from fundamental principles [5]. This brings a validation of our calculations.

C. Circular Birefringence of a Distribution of Helices

Because $\varepsilon_{yz} = 0$ as explained in the appendix, we obtain for a light beam propagating perpendicular to the helix axis direction

$$\Delta\varepsilon_\perp = \frac{i}{2}(\varepsilon_{YZ} - \varepsilon_{ZY}) = -\frac{i}{2}\varepsilon_{zx}, \quad (4.9)$$

whereas it is for a light beam propagating parallel to the helix axis direction

$$\Delta\varepsilon_\parallel = \frac{i}{2}(\varepsilon_{XY} - \varepsilon_{YX}) = -i\varepsilon_{yx}. \quad (4.10)$$

Both expressions can be cast into a unique one:

$$\Delta\varepsilon_{\perp,\parallel} = -\frac{\omega_p^2 E_F n_0}{2 m_e c} \frac{1}{\omega(\omega + i\Gamma)^2} \frac{a^2 b}{L^4} \mathcal{F}_{\perp,\parallel}(ka), \quad (4.11)$$

where $\mathcal{F}_\perp(ka) = -\frac{1}{2}\mathcal{F}(ka)$ and $\mathcal{F}_\parallel(ka) = 1$. Circular birefringence and circular dichroism are obtained from Eqs. (2.25) and (2.26) and, using $k = n_0\omega/c$, read

$$\Delta n_{c\perp,\parallel} = -\frac{\omega_p^2 E_F}{2 m_e c} \frac{a^2 b}{L^4} \mathcal{F}_{\perp,\parallel}(ka) \frac{\omega^2 - \Gamma^2}{\omega(\omega^2 + \Gamma^2)^2}, \quad (4.12)$$

$$\Delta\alpha_{\perp,\parallel} = \frac{\omega_p^2 E_F}{2 m_e c^2} \frac{a^2 b}{L^4} \mathcal{F}_{\perp,\parallel}(ka) \frac{\omega\Gamma}{(\omega^2 + \Gamma^2)^2}. \quad (4.13)$$

For an isotropic distribution of molecules, the relevant dielectric constant is

$$\Delta\varepsilon = \frac{2}{3}\Delta\varepsilon_\perp + \frac{1}{3}\Delta\varepsilon_\parallel, \quad (4.14)$$

which is

$$\Delta\varepsilon = -\frac{\omega_p^2 E_F n_0}{6 m_e c} \frac{1}{\omega(\omega + i\Gamma)^2} \frac{a^2 b}{L^4} [1 - \mathcal{F}]. \quad (4.15)$$

5. DISCUSSION

We would like first to comment on the difference for the parallel and the perpendicular cases. The differences lie in the $\mathcal{F}_\perp$ and $\mathcal{F}_\parallel$ functions, which are plotted in Fig. 2. The most striking difference is that one observes some oscillations in $\mathcal{F}_\perp$, whereas $\mathcal{F}_\parallel$ is constant. This can be understood by considering the inset in Fig. 1, which represents the projection of the helix on a plane perpendicular to its axis. For the parallel case, when the light beam propagates along the helix axis, the polarization plane lies in the figure. As a consequence, the electrons situated at the four points (1), (1′), (2), and (2′) will react in a similar way to the electromagnetic field. Such is not the case when the light beam propagates perpendicular to the axis (say in the (1) – (1′) direction). In that case, the polarization plane is perpendicular to the figure (along the (2) – (2′) line) and the four points do not respond to the same excitation. For points (2) and (2′), the electric field is always perpendicular to the helix and does not provoke any electron motion, whereas for points (1) and (1′), there are components of the electric field parallel to the electronic path. As a consequence, the total response will be sensitive to the relative phase of the electric field between the points (1) and (1′), and one can expect that it will be maximum if the two points are in phase. We therefore expect that the response is maximum when $ka = 0$, as observed in Fig. 2, and displays oscillations with a period $ka = \pi$ in qualitative agreement also with the oscillations observed in Fig. 2. The slight discrepancy as well as the nonperfect periodicity is a consequence of the blurring due to the contributions of all the points of the helix. On the contrary, since all points are equivalent for the parallel case, we do not expect such interference effects and no oscillations are observed in the electronic response.

We want now to examine the frequency dependence of the index and absorption differences [Eqs (4.12) and (4.13)] with the frequency. To do so, we have to take into account the variation of the $\mathcal{F}_\perp$ function as well as of the prefactors. The frequency dependence for Δn_c is $\mathcal{F}(ka)(\omega^2 - \Gamma^2)/(\omega^2 + \Gamma^2)^2$, whereas that for $\Delta\alpha$ is $\mathcal{F}(ka)\omega/(\omega^2 + \Gamma^2)^2$. We have plotted these quantities in Figs. 3 and 4 with the geometrical parameters given above and choosing $\Gamma/2\pi = 6.4$ THz for the copper broadening. The abscissa is given in terahertz. We have plotted the response for the parallel, perpendicular, and isotropic case. Note that the divergence when $\omega \to 0$ is a well-known feature of the Drude model, which can be corrected by many-body calculations such as the Lindhard dielectric function. However, as already pointed out, one can observe that the isotropic quantities go to zero in the small frequency limit due to the fundamental sum rule for Rosenfeld rotational strengths. This means that in the approximation where $a,\ b \ll \lambda$, an isotropic distribution of metallic helices will not give any chiral signal. This surprising result has been known for a long time [16]: the signal coming from helices whose axes are parallel to the wave propagation exactly cancels out the signal coming from helices whose axes are perpendicular to the direction propagation. This can be understood by considering the optical handedness of the system, which for a given geometric handedness is reversed for the two orthogonal propagation directions. However, in the terahertz regime, one can obtain helices for which $a,\ b \ll \lambda$ does not hold and one recovers a chiral signal. Only the full calculation presented here allows this chiral signal to be observed. The usual approximation, which amounts to developing the electric field variation due to propagation across the helices to the first order, is not sufficient to account for this result. As a result, one sees that the optical rotation dispersion as well as the circular dichroism of a random distribution of metallic helices become noticeable for frequencies larger than about 0.5 THz and displays only smooth oscillations connected to the size of the helices. As noted above, the only dimension that plays a role in these oscillations is the helix diameter, but not the pitch.

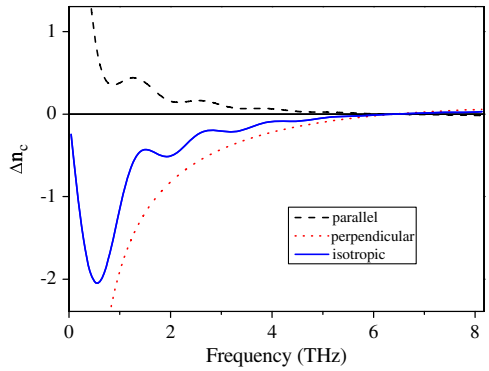

Fig. 3. (Color online) Circular birefringence in arbitrary units as a function of the frequency for helices whose axis is perpendicular (dotted line) and parallel (dashed line) to the beam propagation and for an isotropic distribution of helices (solid line). Note that the isotropic signal goes to 0 when the frequency becomes very small, corresponding to the validity regime of the usual multipolar expansion.

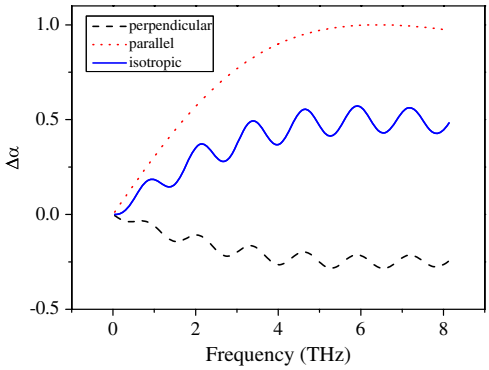

Fig. 4. (Color online) Circular dichroism in arbitrary units as a function of the frequency for helices whose axis is perpendicular (dotted line) and parallel (dashed line) to the beam propagation and for an isotropic distribution of helices (solid line). Note that the isotropic signal goes to 0 when the frequency becomes very small, corresponding to the validity regime of the usual multipolar expansion.

We come now to a numerical estimate of the circular birefringence and dichroism. We stick to the configuration of Chau where a terahertz beam with mean angular frequency equal to $\omega = 2.9 \times 10^{12}$ s^{-1} impinges perpendicularly to the helix axis. A precise estimate is, however, impossible due to the poor knowledge of the numerical values for ω_p and Γ. Γ is especially very badly known as in the literature it goes from 1.38×10^{13} rad/s [17] to 1.45×10^{14} rad/s [18]. We therefore stick to the values proposed in [2] that lie in this range and

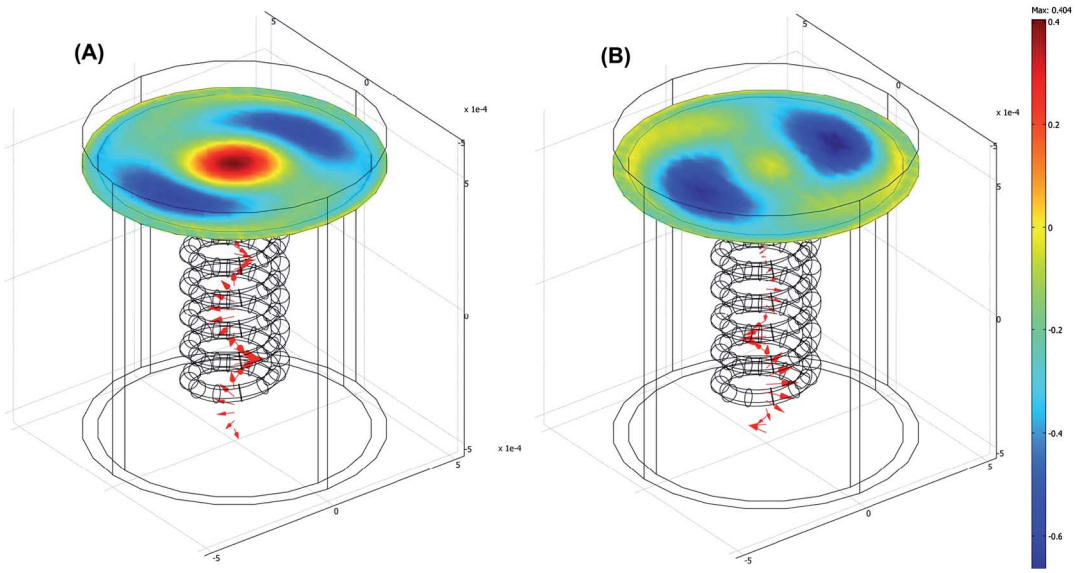

Fig. 5. (Color online) FEM simulations of the optical activity in a metallic helix in the terahertz domain. Color map provides the value of the electric field along the x axis, for right (A) and left (B) incident circular polarizations. The color scale is identical for both polarizations. The red arrows show the electric field direction at the center axis of the helix.

we calculate $\Delta n_c = 0.014$. Using other parameters yield Δn_c comprised between 0.002 and 0.18. These values must be compared to the experimental value $\Delta n_c = 0.043$ [4], which satisfactorily falls between them. We can also comment on the sign of Δn_c, which is negative (resp. positive) for our left-handed helix as soon as $\omega < \Gamma$ as observed in the terahertz regime for a propagation perpendicular (resp. parallel) to the helix axis. This is in accordance with Chau's results since he observed a positive index difference for a right-handed helix [19] with a propagation perpendicular to the axis. As a final remark, we note that the helix parameters mainly come into the above expressions through the factor a^2b/L^4 for estimating the magnitude of the chiral response. On the other hand, note that the terahertz resonance observed in Fig. 2 for the refractive index as well as the oscillations in the circular dichroism (Fig. 3) arise from the function $\mathcal{F}$ whose minima positions are only dependent on the helix radius through the relation $k_{\min}a = 1.9[\pi]$.

6. FINITE ELEMENT CALCULATION

To get another picture of optical activity in metallic helices, we performed numerical simulations. We carried out a direct resolution of Maxwell's equations through a full 3D *ab initio* finite element method (FEM) analysis of the electric field propagating along the helix [20]. This method provides quantitative information on the electric field distribution, allows the calculation of the transmitted terahertz electromagnetic field, and takes into account the helix metal properties. The simulation box is made of a primary cylinder of radius 450 μm and hight 1000 μm, containing the metallic helix. It is radially surrounded by a 50 μm thick perfectly matched layer (PML), which absorbs the incident radiation without producing reflections. PMLs provide good performance for a wide range of incidence angles and are not particularly sensitive to the shape of the wave fronts. On top of the primary cylinder is another 100 μm thick PML plate to avoid back reflection after propagation. The helix is a copper left-handed solid object with cross-section radius 30 μm, radius 150 μm, and distance between turns 120 μm. A total of six turns is used. The helix is surrounded by vacuum. The complex electromagnetic field is calculated in two sets of simulations, for an incident Gaussian wave of right- and left-circular polarizations. The precision of the simulations is controlled by progressively reducing the mesh size, in particular around the helix, until a stationary solution is found. Typical mesh dimensions are $\lambda/5$. The wavelength is 300 μm (1 THz) in vacuum, and the electric conductivity of the helix copper [13] is 5.96×10^7 S/m. Figure 5 shows the value of the electric field along the x axis, for right (A) and left (B) incident circular polarization, in addition with the electric field direction inside the helix (red arrows). From these calculations, we can compute the difference in absorption by integrating Poynting's vector of the entrance and exit boundaries, and we find $\Delta\alpha_c \approx 1.06$ cm^{-1}. The real part of the refractive index can be obtained by calculating the dephasing over propagation. Since the dephasing is expected to be less than π, the real part is given by $\Delta n_c = \frac{\Delta\phi\lambda}{2\pi l}$, where $\Delta\phi = \phi_L - \phi_R$ is the phase difference between left and right polarization, and l is the thickness of the helix. Here, $l = 720$ μm. We find $\Delta\phi = 0,35$, so $\Delta n_c = 0.023$. Here again, the order of magnitude is excellent. Plugging the parameters of the calculation in Eqs (4.12) and (4.13) for the parallel case and using [2] for the copper parameters, we find that $\Delta n_c = 0.011$ and $\Delta\alpha_c = 1.2$ cm^{-1}. Note that Δn_c and $\Delta\alpha_c$ have the same sign, in accordance with our calculation when $\omega < \Gamma$. We note also that the sign of Δn_c is positive as expected for a propagation parallel to the axis of a left-handed helix.

7. CONCLUSION

In this article, we have been interested in the microscopic origin of the circular birefringence and dichroism of a metallic helix in the terahertz regime. In this regime where the electromagnetic wavelength is comparable to the geometrical dimensions of the system, one cannot use the usual and convenient multipolar development, but one must carry out a complete nonlocal calculation of the light–matter interaction. We have analytically performed such a calculation for two limiting

cases, namely for a light propagation perpendicular or parallel to the helix axis. The final expressions are very tractable and allow one to obtain the circular birefringence and dichroism for an assembly of helices fully aligned or for an isotropically distribution.

Several outcomes have been obtained. First, from a fundamental view point, it is interesting to observe that the overall chiral effect for an isotropic distribution of helices completely vanishes in the commonly used multipolar development: the effects of helices whose axes are perpendicular to the beam propagation exactly cancel out the effects of helices whose axes are parallel to the beam propagation. Such is not the case in the fully nonlocal calculation where the two contributions have different frequency dependence. The analytical formula also shows that no sharp resonance is expected when the light wavelength is changed. Only smooth oscillation is observable when the axis is perpendicular to the light propagation and no special feature is observed in the other configuration, the relevant geometrical factor being the helix radius and not its pitch.

We have also been able to give a numerical estimate of the expected circular birefringence and we have been able to obtain very good qualitative agreement with the experimental values measured by Chau, limited by the large uncertainty on the numerical value of the relaxation frequency.

Finally, as a complementary check of the relevance of our results, we have carried out a finite element simulation of the system and we have also obtained a numerical value for the circular birefringence in good agreement with the theoretical calculation and with the experiment.

The fully theoretical calculation presented here has the advantage to give a clear microsopic insight into the underlying phenomena. On the other hand, the finite element calculation fully solves the Maxwell equations numerically but only gives phenomonological results. We think that thanks to the complementarity of the two techniques, we have achieved a thorough understanding of the optical activity of a metallic helix in the terahertz spectral range.

APPENDIX A: CALCULATION OF A_{nm}, B_{nm}, C_{nm}, AND $\sum (F_m - F_n)C_{nm}\omega_{nm}$

In this and the following appendices, we calculate the various matrix elements and their combinations, which enter the general formula of the dielectric constants [see Eqs. (4.3) and (4.7)].

Let us first consider

$$A_{nm} = \langle n|e^{iky}\widehat{p}_x|m\rangle. \tag{A1}$$

Let us recall that in the local approximation where $ky \ll 1$, this factor reduces to the usual matrix element of the momentum operator. This quantity is therefore the nonlocal extension of this momentum operator component, which describes the light–matter interaction in a very general way. We have

$$\begin{aligned} A_{nm} &= i\frac{\hbar a}{L^2}\frac{1}{K\pi}\int_0^{2K\pi} \sin n\theta e^{ika\sin\theta} \\ &\quad\times\left[\sin\theta\frac{\partial}{\partial\theta}+\frac{1}{2}\cos\theta\right]\sin m\theta \mathrm{d}\theta \\ &= i\frac{\hbar a}{8L^2}[(2m-1)(F_{n+m-1}-F_{n-m+1}) \\ &\quad+(2m+1)(F_{n-m-1}-F_{n+m+1})], \end{aligned} \tag{A2}$$

where

$$F_M = \frac{1}{K\pi}\int_0^{2K\pi} e^{ika\sin\theta}\cos M\theta. \tag{A3}$$

Calculation of this integral can be carried out with the help of the following identity:

$$e^{iz\sin\theta} = \sum_{n=-\infty}^{+\infty} e^{in\theta}J_n(z), \tag{A4}$$

where J_n is the Bessel function of order n. We obtain the following:

- If M is an integer number, then $F_M = J_M(ka) + J_{-M}(ka) = 2J_M(ka)$ if M is even, and 0 if M is odd.
- If M is not an integer number, F_M is not necessarily null, but it varies as $\frac{1}{K}$ when $K \to \infty$. We will therefore neglect these terms (long helix).

This means that the states $|n\rangle$ and $|m\rangle$ will give a nonzero contribution to A_{nm} on the condition that $n \pm m \pm 1$ is an even integer number. Note that the Bessel functions J_M for arguments of the order of 1 decrease very strongly when M increases. We have seen that n and m are very large numbers and therefore only Bessel functions of order $n - m \pm 1$ with $n \approx m$ will give nonnegligible contributions, whereas those of order $n + m \pm 1$ can be neglected. Therefore

$$\begin{aligned} A_{nm} &= i\frac{\hbar a}{4L^2}[2m[J_{n-m-1}(ka) - J_{n-m+1}(ka)] \\ &\quad+[J_{n-m-1}(ka) + J_{n-m+1}(ka)]] \\ &= i\frac{\hbar a}{L^2}[mJ'_{n-m}(ka) + \frac{n-m}{2ka}J_{n-m}(ka)], \end{aligned} \tag{A5}$$

where J' is the derivative of J. This yields

$$A_{nm} + (\tilde{A}_{mn})^* = -i\frac{\hbar a}{L^2}(n+m)J'_{n-m}(ka). \tag{A6}$$

Performing an identical calculation for $A'_{nm} = \langle n|e^{ikx}\widehat{p}_y|m\rangle$ yields 0, implying that $\varepsilon_{yz} = 0$.

Similarly, we can calculate B_{nm}

$$\begin{aligned} B_{nm} &= \langle n|e^{-iky}\widehat{p}_z|m\rangle \\ &= -i\frac{\hbar b}{L^2}\frac{1}{K\pi}\int_0^{2K\pi} \sin n\theta e^{-ika\sin\theta}\frac{\partial}{\partial\theta}\sin m\theta \ \mathrm{d}\theta \\ &= -i\frac{\hbar b}{L^2}\frac{m}{2}(G_{n+m}+G_{n-m}), \end{aligned} \tag{A7}$$

where

$$G_M = \frac{1}{K\pi}\int_0^{2K\pi} e^{-ika\sin\theta}\sin M\theta. \tag{A8}$$

With the same reasoning as previously, we obtain than G_M can be neglected as soon as M is not an integer number. If M is an odd integer, $G_M = -2iJ_M(ka)$, it is null if M is even.

Here again, we see that the states $|n\rangle$ and $|m\rangle$ will give a nonzero contribution to B_{nm} on the condition that $n \pm m$

be an odd integer number, which is equivalent to the condition for a nonzero A_{nm}. With the same approximation as before, we obtain

$$B_{nm} = \frac{\hbar b}{L^2} m J_{n-m}(ka) \tag{A9}$$

and

$$B_{nm} + (\tilde{B}_{mn})^* = -\frac{\hbar b}{L^2}(n+m) J_{n-m}(ka). \tag{A10}$$

With the above formula, one readily obtains

$$C_{nm} = -i\frac{\hbar^2 ab}{L^4}(n+m)^2 J'_{n-m}(ka) J_{n-m}(ka) \tag{A11}$$

and we can check that $C_{nm} = C_{nm}$.

We want now to calculate

$$I_C = \sum_{m,n}(f_m - f_n) C_{nm}\omega_{nm}. \tag{A12}$$

We have

$$\omega_{nm} = (n^2 - m^2)E_0 \simeq 2m_F l, \tag{A13}$$

where we have defined $l = n - m > 0$ and use the relation $n \simeq m \simeq m_F$. We can therefore write

$$I_C = -i\frac{\hbar^2 ab}{L^4} E_0 \times 8m_F^3 \sum_m (f_m - f_{m+l}) \sum_{l\,\mathrm{odd}} l J'_l(ka) J_l(ka). \tag{A14}$$

The summation over m can be written ($l \ll m_F$)

$$\sum_m (f_m - f_{m+l}) = -l\sum_m \frac{\partial f}{\partial m} = 4Kl, \tag{A15}$$

whatever the temperature T. The factor $4K$ comes from the state counting (remembering that $2Km = p$ with p an integer number), including the spin degeneracy. This temperature independence is only valid as long as the above first-order development is valid. We finally obtain

$$I_C = -i2N\frac{\hbar^2 kab}{L^4} E_F \mathcal{F}(ka) \tag{A16}$$

with $\mathcal{F}(x) = \frac{4}{x}\sum_{l\,\mathrm{odd}} l^2 J'_l(x) J_l(x)$.

APPENDIX B: CALCULATION OF D_{nm}, E_{nm}, F_{nm}, AND $\sum (F_m - F_n) F_{nm}\omega_{nm}$

We have

$$\begin{aligned} D_{nm} &= \langle n|e^{ikz}\widehat{p}_x|m\rangle \\ &= i\frac{\hbar a}{L^2}\frac{1}{K\pi}\int_0^{2K\pi} \sin n\theta\, e^{ikb\theta}\left[\sin\theta\frac{\partial}{\partial\theta} + \frac{1}{2}\cos\theta\right]\sin m\theta \mathrm{d}\theta \\ &= i\frac{\hbar a}{8L^2}[(2m-1)(H_{n+m-1} - H_{n-m+1}) \\ &\quad + (2m+1)(H_{n-m-1} - H_{n+m+1})], \end{aligned} \tag{B1}$$

where

$$\begin{aligned} H_M &= \frac{1}{K\pi}\int_0^{2K\pi} e^{ikb\theta}\cos M\theta \mathrm{d}\theta \\ &= \frac{1}{2K\pi}\int_0^{2K\pi}[e^{i(kb+M)\theta} + e^{i(kb-M)\theta}]\mathrm{d}\theta. \end{aligned} \tag{B2}$$

For a long helix, $\frac{1}{2K\pi}\int_0^{2K\pi} e^{i(kb\pm M)\theta}\mathrm{d}\theta$ can be approximated by $\delta(kb \pm M)$, where δ is the Kronecker symbol. Let us recall that n and m are real numbers that can assume almost any value when $K \gg 1$.

The calculation of E_{nm} is identical:

$$\begin{aligned} E_{nm} &= \langle n|e^{-ikz}\widehat{p}_y|m\rangle = -i\frac{\hbar a}{L^2}\frac{1}{K\pi}\int_0^{2K\pi} \sin n\theta^{-ikb\theta} \\ &\quad \times\left[\cos\theta\frac{\partial}{\partial\theta} - \frac{1}{2}\sin\theta\right]\sin m\theta \mathrm{d}\theta \\ &= i\frac{\hbar a}{8L^2}[(2m-1)(I_{n+m-1} + I_{n-m+1}) \\ &\quad + (2m+1)(I_{n-m-1} + I_{n+m+1})], \end{aligned} \tag{B3}$$

where

$$\begin{aligned} I_M &= \frac{1}{K\pi}\int_0^{2K\pi} e^{-ikb\theta}\sin M\theta \mathrm{d}\theta \\ &= \frac{1}{2iK\pi}\int_0^{2K\pi}[e^{i(-kb+M)\theta} - e^{i(-kb-M)\theta}]\mathrm{d}\theta. \end{aligned} \tag{B4}$$

In these expressions, we have $kb \ll m, n$. We therefore keep only the δ's involving $n - m$ (which can be very small) and neglect all δ's involving $n + m$, which can never be of the order of kb. Finally, we can calculate F_{nm} and we obtain

$$\begin{aligned} F_{nm} &= i\left(\frac{\hbar a}{L^2}\right)^2 \frac{1}{16}(n+m)^2[\delta(l+kb+1) - \delta(l-kb+1) \\ &\quad - \delta(l+kb-1) + \delta(l-kb-1)]. \end{aligned} \tag{B5}$$

The summation $I_F = \sum F_{nm}\omega_{nm}$ can be written

$$\begin{aligned} I_F &= i\frac{\hbar^2 a^2}{16L^4} E_0 \times 8m_F^3 \sum_m (f_m - f_{m+l}) \\ &\quad \times \sum_l [\delta(l+kb+1) - \delta(l-kb+1) \\ &\quad - \delta(l+kb-1) + \delta(l-kb-1)]. \end{aligned} \tag{B6}$$

Remembering that $kb > 0$, the summation, here again temperature-independent at first order reduces to $8K\,kb$, and we obtain

$$I_F = 2iN\frac{\hbar^2 ka^2 b}{L^4} E_F. \tag{B7}$$

REFERENCES

1. D. Mittleman, *Sensing with Terahertz Radiation*, *Optical Sciences* (Springer, 2003).
2. K. J. Chau, M. C. Quong, and A. Y. Elezzabi, "Terahertz time-domain investigation of axial optical activity from a subwavelength helix," Opt. Express **15**, 3557–3567 (2007).
3. A. Y. Elezzabi and S. Sedergberg, "Optical activity in an artificial chiral media: a terahertz time-domain investigation of Karl F. Lindman's 1920 pioneering experiment," Opt. Express **17**, 6600–6612 (2009).

4. K. J. Chau, "Investigation of the chiral origins of electromagnetic activity," Opt. Lett. **35**, 1187–1189 (2010).
5. L. Barron, *Molecular Light Scattering and Optical Activity*, 2nd ed. (Cambridge University, 2004).
6. I. Tinoco, "Circular dichroism of large molecules," Int. J. Quantum Chem. **16**, 111–117 (1979).
7. L. D. Landau and E. M. Lifchitz, *Electrodynamics of Continuous Media*, 2nd ed. (Pergamon, 1984).
8. D. M. Wood and N. W. Ashcroft, "Quantum size effects in the optical properties of small metallic particles," Phys. Rev. B **25**, 6255–6274 (1982).
9. D. Moore and I. Tinoco, "The circular dichroism of large helices. A free particle on a helix," J. Chem. Phys. **72**, 3396–3400 (1980).
10. M. G. Silveirinha, "Metamaterial homogenization approach with application to the characterization of microstructured composites with negative parameters," Phys. Rev. B **75**, 115104 (2007).
11. M. Born and E. Wolf, *Principles of Optics*, 6th ed. (Cambridge University, 1997).
12. D. J. Griffiths, *Introduction to Electrodynamics* (Prentice Hall, 1999).
13. *Handbook of Chemistry and Physics*, 76th ed. (CRC Press, 1996).
14. F. Hache, D. Ricard, and C. Flytzanis, "Optical nonlinearities of small metal particles: surface-medited resonance and quantum-size effect," J. Opt. Soc. Am. B **3**, 1647–1655 (1986).
15. B. B. Dasgupta and R. Fuchs, "Polarizability of a small sphere including nonlocal effects," Phys. Rev. B **24**, 554–561 (1981).
16. E. U. Condon, "Theories of optical rotatory power," Rev. Mod. Phys. **9**, 432–457 (1937).
17. M. A. Ordal, R. J. Bell, R. W. Alexander, L. L. Long, and M. R. Querry, "Optical properties of fourteen metals in the infrared and far infrared: Al, Co, Cu, Au, Fe, Pb, Mo, Ni, Pd, Pt, Ag, Ti, V, and W," Appl. Opt. **24**, 4493–4499 (1985).
18. E. J. Zeman and G. C. Schatz, "An accurate electromagnetic study of surface enhancement factors for Ag, Au, Cu, Li, Na, Al, Ga, In, Zn, and Cdv," J. Phys. Chem. **91**, 634–643 (1987).
19. Note that the sign of Δn_c is not made explicit in [4] but it can be inferred from its Fig. 2.
20. Comsol multiphysics 3.4 (Comsol, Sweden).